Materials Horizons

COMMUNICATION

Cite this: *Mater. Horiz.*, 2019, 6, 318

Received 4th January 2018,
Accepted 18th October 2018

DOI: 10.1039/c8mh00019k

rsc.li/materials-horizons

Giant spontaneous exchange bias in an antiperovskite structure driven by a canted triangular magnetic structure†

Lei Ding, ‡*[a] Lihua Chu,‡[b] Pascal Manuel,*[a] Fabio Orlandi,[a] Meicheng Li,[b] Yanjiao Guo[b] and Zhuohai Liu[b]

Exchange bias (EB) effect, generally observed in systems consisting of ferromagnetic and antiferromagnetic layers after a cooling procedure in a high magnetic field, is highly desirable for technological applications ranging from spintronics to magnetic recording. Achieving a giant EB effect near room temperature in a small cooling field is thus an on-going technologically relevant challenge for the materials science community. In this work, we present the experimental realization of such a fundamental goal by demonstrating the existence of giant EB after a zero field cooled (ZFC) procedure in antiperovskite $Mn_{3.5}Co_{0.5}N$ below 256 K. We found that it exhibits an EB field of −0.28 T at 50 K after a ZFC procedure accompanied by a large vertical magnetization shift (VMS). Interestingly, this EB field can be elevated up to −1.2 T after a cooling procedure with a small applied field of just 500 Oe. $Mn_{3.5}Co_{0.5}N$ represents the first intermetallic material showing a strong correlation between EB and VMS. We attribute the observed EB effect to a new canted triangular magnetic structure in antiperovskites determined by a neutron diffraction experiment. Finally, we discuss the striking effect of Co substitution on the physical properties of antiperovskite materials and put forward a new strategy for the antiperovskite lattice to exploit new single phase materials showing large EB effect at room temperature.

Conceptual insights

Exchange bias (EB) has significantly accelerated the ever-increasing density of magnetic recording devices and promoted the development of spintronics. In the past few decades, the quest for these applications has stimulated intensive studies to search for and design materials with large EB near room temperature. However, a conventional EB effect usually requires a large magnetic cooling field to obtain a considerable EB field. By contrast, a novel phenomenon is the so-called spontaneous EB effect where a large EB field can be generated without a cooling field. Antiperovskite compounds with triangular lattices provide a perfect platform for the design of multifunctional materials as they can incorporate a wide range of elements, leading to a variety of physical properties. In this work, we found that a giant EB effect emerges in a new antiperovskite $Mn_{3.5}Co_{0.5}N$ when subjected to a small or even null cooling field. Such a phenomenon is attributed to a new triangular magnetic structure in sharp contrast to the previously reported EB in bulk materials, where the mechanisms are always related to heterogeneous features such as spin-glass or magnetic phase separation. These findings lay out a new route for obtaining a large EB field in the presence of a null or small cooling field in bulk materials. By exploiting the magnetic features of antiperovskite triangular lattices, we put forward that the suppression of the exchange interactions between the two magnetic sublattices in the Mn_4N lattice is a key ingredient for the occurrence of a large EB effect around room temperature. We also proposed a promising route for experimentally probing this concept in both bulk and thin film systems based on antiperovskite lattices.

1 Introduction

Exchange bias (EB),[1,2] which is characterized by a shift of the hysteresis loop along the field axis in materials composed of ferromagnetic (FM) and antiferromagnetic (AFM) layers, possesses significant technological applications in advanced magnetic devices such as spin valves, magnetic tunnel junctions and magnetoresistive sensors.[3–10] It is conventionally generated by a unidirectional exchange anisotropy when the material is cooled in a static magnetic field below the AFM transition.[10–16] A simultaneous but rarely observed effect is a shift in the magnetic hysteresis loop along the magnetization axis, which is referred to as a vertical magnetization shift (VMS).[17–20] Recently, the VMS effect has been observed in several magnetic bilayer systems, in which it seems to be an effective source for the exchange bias effect.[17,18]

Since the first observation of exchange bias in Co/CoO systems, a large number of investigations have been devoted

[a] *ISIS Facility, Rutherford Appleton Laboratory, Harwell Oxford, Didcot, OX11 0QX, UK. E-mail: lei.ding.ld@outlook.com, lei.ding@stfc.ac.uk, pascal.manuel@stfc.ac.uk*

[b] *State Key Laboratory of Alternate Electrical Power System with Renewable Energy Sources, School of Renewable Energy, North China Electric Power University, Beijing 102206, China*

† Electronic supplementary information (ESI) available. See DOI: 10.1039/c8mh00019k

‡ These authors contributed equally to this work.

to the study of EB in nanostructures and heterostructures to develop advanced magnetic materials for practical applications and to microscopically understand it.[7–16] The vast majority of the investigated cases are heterogeneous systems characterized by magnetic phase separations at low temperature.[19,21–24] By contrast, the EB effect in single phase bulk materials is less exploited.[19] As a representative system, Heusler Mn–Pt–Ga has been found to show giant EB higher than 3 T at 5 K after a cooling field of 10 T due to the formation of FM clusters mixed in a ferrimagnetic (FIM) host.[24] Nevertheless, such a giant effect in Heusler Mn–Pt–Ga, occurring at low temperature and requiring a cooling field of 10 T, impedes its practical applications.

Remarkably, the observation of the EB effect under the application of a zero field cooled (ZFC) procedure, also known as the spontaneous exchange bias effect, is less common. Wang *et al.* first reported such a phenomenon in the Ni–Mn–In Heusler system,[16] and later on, it was also disclosed in other intermetallic systems.[21–24] This effect was explained in terms of a magnetic phase separation between superferromagnetic and AFM regions, in which the strong uniaxial anisotropy needed for the EB effect can be accomplished isothermally without a field-cooled (FC) procedure.

Therefore, the long-standing goal is the quest for giant EB materials, which can operate over a wide temperature range up to room temperature when subjected to a relatively small or even null cooling magnetic field. In the present work we suggest a new route to achieve this goal by exploiting the magnetic features of the antiperovskite triangular lattice.

Mn-Based antiperovskite compounds with formula Mn_3AX (A = Mn, Ni, Cu, Zn, Ga, Ge, *etc.*; X = carbon or nitrogen) have attracted great interest as they exhibit a wide variety of novel physical properties, such as negative thermal expansion (NTE),[25–32] near-zero temperature coefficient of resistivity,[33] spin glass behavior[34] and barocaloric effect.[35] Most antiperovskite compounds crystallize in space group $Pm\bar{3}m$, as shown in Fig. 1, with the magnetic Mn atoms located at the face-centered site, the A atoms at the corner site, and the X atoms at the body-centered site. This arrangement gives rise to a triangular lattice composed of magnetic Mn atoms at the face-centered sites (Fig. 1), leading to geometrical frustration. Previous investigations have revealed that all the intriguing properties of Mn-based antiperovskites are attributed to a noncollinear AFM spin configuration on the triangular lattice.[25–28] When the corner position of the cubic cell is partially occupied by Mn atoms, novel magnetic properties are expected since one extra magnetic position is involved.[31,36] For example, Invar-like behavior has been revealed in $Mn_{3+x}Ni_{1-x}N$ due to the coexistence of FM and typical triangular AFM phases.[36]

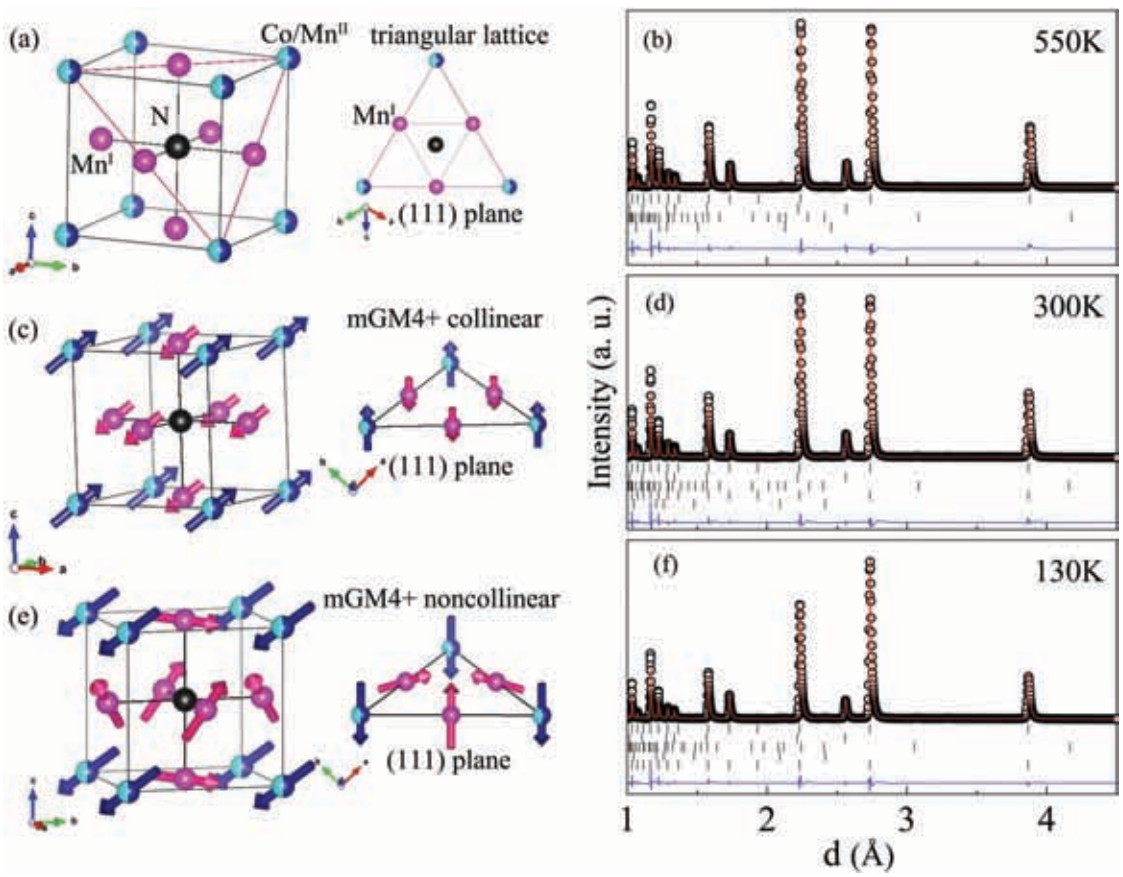

Fig. 1 (a, c and e) Nuclear and magnetic structures for $Mn_{3.5}Co_{0.5}N$ at 550, 300 and 130 K, respectively. (b, d and f) Observed (open circles) and calculated (line) neutron powder diffraction patterns for $Mn_{3.5}Co_{0.5}N$ collected at 550, 300 and 130 K. The nuclear reflections are denoted by upper tick marks. The reflections marked in the middle belong to impurity phases MnO (3.5(3) wt%), Mn_2N (0.86(5) wt%) and CoO (0.32(4) wt%). The lowest tick marks show magnetic reflections. The bottom line stands for the difference between the observed and calculated patterns.

In this work, we investigate the structural and magnetic properties of $Mn_{3.5}Co_{0.5}N$. For the first time, we observed considerable VMS below T_N = 256 K under both FC and ZFC conditions in a magnetic single phase intermetallic system. The VMS, related to the net magnetic moment in a nearly compensated FIM, leads to a large EB effect under ZFC conditions. Moreover, the value of the EB field can remarkably be increased by applying a small cooling field. The possible mechanism governing this interesting phenomenon is discussed based on the experimentally determined magnetic and nuclear structures.

2 Results

The synthesis of the compound has been performed using a standard solid state reaction method. Powders of the reactants Mn_2N and Co were mixed and pressed into pellets. The pellets were then wrapped in Ta foil to prevent oxidation and to capture the N_2 released during the reaction avoiding the formation of nitride impurities. Synthesis performed with Au foil yielded highly oxidized materials as demonstrated in the ESI.† The synthesis conducted with stoichiometric amounts of the reactants, targeting the composition $Mn_{3.5}Co_{0.5}N$, results in a high concentration of Mn_2N in the final material, indicating Co as the limiting reagent. Attempts with an excess of Co were then carried out in order to improve the purity of the final material. As summarized in Table S1, in the ESI,† the best quality samples were achieved when a 110 wt% excess of Co powder was used. No trace of Co was found in the final material but a small amount of CoO impurity (0.32(4) wt%) was detected by neutron diffraction (see Fig. S1, ESI†). However, EDX and XRD measurements performed on the Ta foil and on the quartz tube surface reveal the formation of $CoTa_2$ which explains the high Co losses during the reaction. We present in the main text the results obtained on the sample synthesized with a 110 wt% Co excess, whereas magnetization and neutron measurements performed on other samples synthesized with different amounts of Co excess are reported in the ESI† (see Fig. S7–S9). It is worth noting that the magnetic properties are very similar in all the investigated samples. In particular, Rietveld refinement of the neutron diffraction data, taking advantage of the good contrast between Co and Mn, always returns the same composition for the main phase, namely $Mn_{3.5}Co_{0.5}N$ (Table S2, ESI†). These observations suggest that the detected physical properties are indeed intrinsic to the $Mn_{3.5}Co_{0.5}N$ compound.

As shown in Fig. 1, neutron powder diffraction indicates that $Mn_{3.5}Co_{0.5}N$ crystallizes in an antiperovskite cubic structure with $Pm\bar{3}m$ symmetry, in which Mn(I) and N reside on the 3c and 1b Wyckoff positions, respectively, whereas the 1a position is occupied by half Co and half Mn(II). Therefore the chemical formula could be written as $Mn^{I}_{3}Mn^{II}_{0.5}Co_{0.5}N$. The corresponding results from Rietveld refinement including the fractional occupation of Mn and Co are presented in Table S3 in the ESI.† While temperature-dependent neutron diffraction in the temperature range of 8–550 K does not show a structural symmetry change, a large NTE was observed from 220 to 260 K,

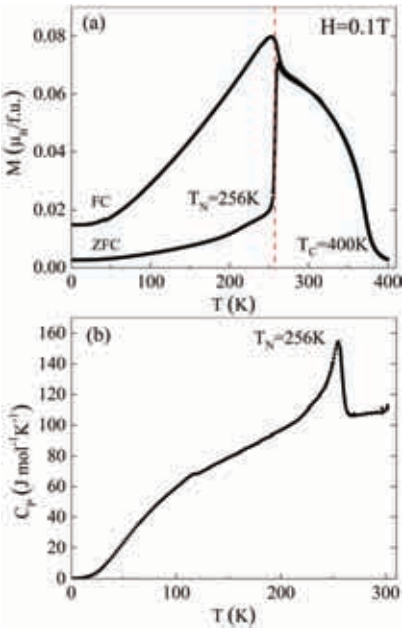

Fig. 2 (a) Temperature dependence of the magnetization of $Mn_{3.5}Co_{0.5}N$ measured with ZFC and FC conditions under 0.1 T from 2 to 400 K. (b) Heat capacity of $Mn_{3.5}Co_{0.5}N$ in the temperature range of 5–300 K. A very small cusp at 115 K represents the contribution from MnO.

accompanied by a magnetic phase transition at T_N = 256 K (Fig. S11, ESI†). In sharp contrast to other antiperovskites, where NTE is usually associated with the so-called mGM5+ AFM magnetic structure,[25–28] we found that the NTE in $Mn_{3.5}Co_{0.5}N$ is in fact related to a more complex magnetic configuration transformed by mGM4+, as explained below.

Fig. 2(a) shows the temperature dependence of the magnetization of $Mn_{3.5}Co_{0.5}N$, measured at 0.1 T under both ZFC and FC conditions. Two magnetic phase transitions are clearly seen: upon cooling, it first undergoes a FIM transition at T_C = 400 K (determined by our temperature-dependent neutron diffraction), then an AFM transition sets in at T_N = 256 K. The irreversibility between ZFC and FC curves reflects the presence of a weak FM component below T_N. Specific heat from 2 to 300 K further supports the presence of an AFM transition at 256 K (Fig. 2(b)). A small cusp at 115 K in the heat capacity is attributed to the small amount of MnO impurity.

The magnetic hysteresis loops of $Mn_{3.5}Co_{0.5}N$ were measured over a temperature range of 5–300 K under ZFC conditions, giving particular care to eliminate any small trapped magnetic field in the SQUID at 400 K. The measurements, shown in Fig. 3, were recorded between −7 T and 7 T using the protocol: 0 → 7 T → 0 → −7 T → 0 → 7 T. The hysteresis loops measured below T_N, seen in Fig. 3(a), show the occurrence of large horizontal and vertical shifts under ZFC conditions. In particular, these shifts make the loops asymmetric at 50 K, entailing a giant EB field of −0.28 T. The H_{EB} and vertical magnetization shift M_{shift} are defined as $H_{EB} = (H_L + H_R)/2$ and $M_{shift} = (M^+ + M^-)/2$, respectively, where H_L and H_R are the left and right coercive fields, and M^+ and M^- are the maximum positive and negative magnetization[20] (see the marks in Fig. 4(c)). The temperature

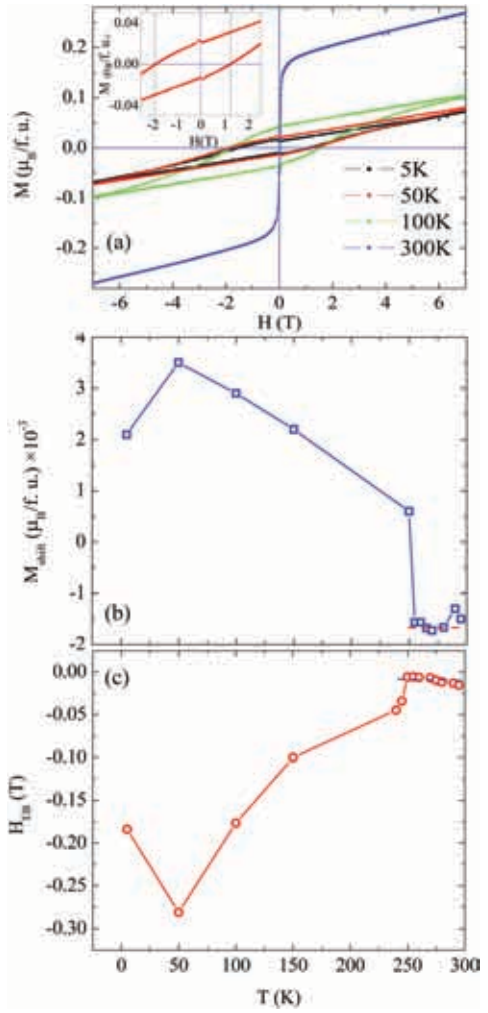

Fig. 3 (a) Magnetic hysteresis loops of $Mn_{3.5}Co_{0.5}N$ at different temperatures under ZFC conditions. Inset shows the enlargement of the magnetic hysteresis loop at 50 K. (b) and (c) Temperature dependence of the H_{EB} and M_{shift} under ZFC conditions.

evolution of H_{EB} and M_{shift} is presented in Fig. 3(b and c), showing that a large value of M_{shift} always accompanies large negative H_{EB}. Note that the large EB occurs in the vicinity of T_N, ruling out the contribution of a tiny amount of the impurity phase CoO (AFM below 290 K) and MnO (AFM below 115 K). Several repeated measurements of the hysteresis loop at 5 K under ZFC conditions always exhibit a small drop in the EB field from 50 to 5 K.

Fig. 4 shows the hysteresis loop measured under field-cooled conditions, together with the field and temperature dependence of the H_{EB} and M_{shift}. One can immediately see that the robust EB effect occurs only below 250 K, again excluding the influence of impurity phases CoO and MnO. In accordance with the ZFC measurements, the latter two quantities are strictly related: as the VMS changes from 7.5% at 200 K to 23% at 50 K, the absolute value of H_{EB} rises typically from 0.22 T to 1 T. The maximum H_{EB} is 1.2 T at 5 K under a cooling field of only 0.1 T. In order to further study the giant EB effect, we have investigated its cooling field dependence in the magnetic field range 0.005–5 T (results measured under high fields are shown in Fig. S12–S16, ESI†). It is evident that the value of H_{EB} increases rapidly with increasing cooling field (H_{CF}) and saturates to 1.2 T above H_{CF} = 500 Oe (see Fig. 4(d) and Fig. S12, ESI†). M_{shift} rapidly increases accordingly and reaches its maximum under a cooling field of 0.1 T (see Fig. 4(d)). This feature makes $Mn_{3.5}Co_{0.5}N$ clearly distinct from the documented magnetic phase-separated oxides, and super spin glassy or cluster glassy alloys, where H_{EB} typically decays rapidly with a high cooling field, known as a minor loop effect.[19]

It is well known that one of the interesting characteristics in exchange bias materials is the so-called training effect, which describes the monotonous decrease of an exchange-bias field with the cycling index number N. Fig. 5 shows the training effect, measured up to N = 10, in $Mn_{3.5}Co_{0.5}N$ at 5 and 150 K after a FC procedure with an applied field of 1 T. At both temperatures, the decrease of H_{EB} between the first and second loops is evident (H_{EB} reduces by 19% at 5 K) while from the second to the tenth loop H_{EB} is slightly and gradually reduced. Such a relaxation feature is more clear in Fig. 5(b) and (d) which shows H_{EB} as a function of cycling index number N. The decrease of H_{EB} as a function of N ($N > 1$) follows the empirical power law:

$$H_{EB} - H_{EB}^{\infty} \propto \frac{1}{\sqrt{N}} \quad (1)$$

where H_{EB}^{∞} is the exchange-bias field in the limit of infinite loops. The power-law fit yields H_{EB}^{∞} = −0.93 T and −0.18 T for cycles at 5 and 150 K, respectively.

Our neutron diffraction data are consistent with the magnetic susceptibility and heat capacity results, indicating the onset of long-range magnetic ordering below the relevant critical temperatures T_C and T_N. Below 400 K, an enhancement of the nuclear reflections 100 and 110 is observed, whereas neutron diffraction patterns below 260 K indicate an increase of the 110 and 210 reflections. The two sets of magnetic reflections can be indexed by a propagation vector $\mathbf{k}$ = 0. For both magnetic phases, the best fit was achieved with the model described by the mGM4+ irreducible representation.[37–39] The refined neutron patterns and the corresponding illustrations of magnetic structures are shown in Fig. 1. The collinear magnetic structure at 300 K consists of ferromagnetically aligned Mn^{II}/Co spins (1.20(2)μ_B) along the easy axis direction [111] and antiparallel Mn^{I} spins (0.15(5)μ_B), giving rise to a net magnetic moment of 0.75μ_B. In fact, this magnetic configuration is the same as the parent compound Mn_4N.[40] By contrast, the magnetic structure at 130 K is more complex as it is characteristic of the canted noncollinear AFM sublattice arrangement of Mn^{I} spins, which is partially compensated by ferromagnetically ordered Mn^{II} (Fig. 1(e)). The refined moments at 130 K for Mn^{I} and Mn^{II} are 1.70(6) and 4.4(1)μ_B, respectively.

3 Discussion

Let us discuss possible mechanisms underpinning this novel EB in $Mn_{3.5}Co_{0.5}N$. The phenomenological model, generally adopted for EB in heterostructures, where the uncompensated AFM spins pin the interfacial FM ones through exchange

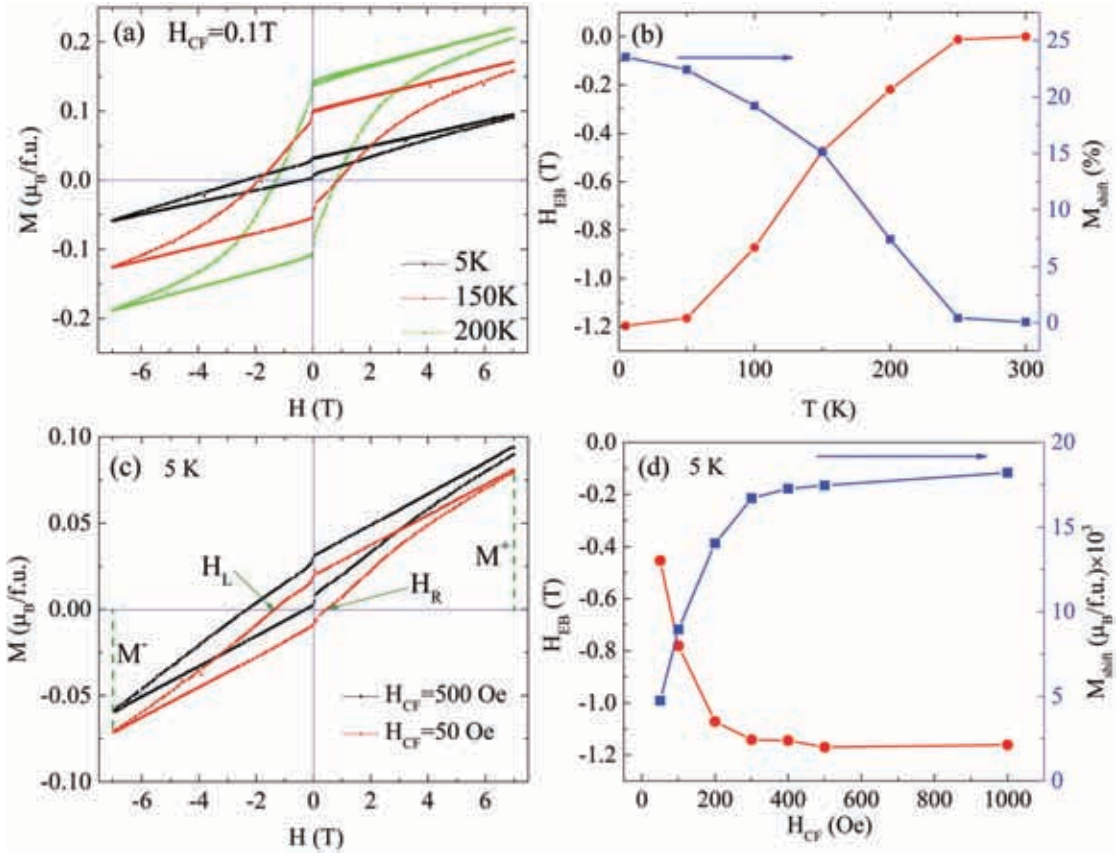

Fig. 4 (a) Magnetic hysteresis loops of $Mn_{3.5}Co_{0.5}N$ at different temperatures under a cooling field of 0.1 T. (b) Temperature dependence of the H_{EB} and M_{shift} under a cooling field of 0.1 T. (c) Magnetic hysteresis loops of $Mn_{3.5}Co_{0.5}N$ at 5 K under cooling fields of 50 and 500 Oe. (d) Cooling-field dependence of H_{EB} and M_{shift} at 5 K.

coupling, is clearly not applicable to $Mn_{3.5}Co_{0.5}N$. The EB effect in several alloys and intermetallics has previously been explained by a magnetic phase separation or a spin glass in materials such as Fe_2MnGa, Mn_2FeGa and $Mn_{50}Ni_{42}Sn_8$.[41–43] As mentioned above, a common phenomenon in these systems, which is absent in $Mn_{3.5}Co_{0.5}N$, is the minor loop effect, implying a different mechanism with respect to previous studied systems. The FM cluster mechanism in the Heusler Mn–Pt–Ga system should also be ruled out since we did not observe any clear change in the irreversibility between ZFC and FC $M(T)$ curves with an increasing field (Fig. S17, ESI†), or any diffuse scattering contribution in the neutron data indicative of short-range ordering as expected in the case of FM clustering or spin glass behavior.[24] A similar cooling-field dependence behavior was recently observed in $YMn_{12-x}Fe_x$ and $YbFe_2O_4$ where global interactions between FM and AFM sublattices are thought to be responsible for their EB effects.[23,44] However, they do not display the VMS effect, which is significant in producing EB in $Mn_{3.5}Co_{0.5}N$, and never observed in an intermetallic system before.

We propose that the giant EB in $Mn_{3.5}Co_{0.5}N$ originates from the global interaction between two magnetic sublattices rather than the interfacial exchange coupling. To set up a qualitative model, it is instructive to take into account the magnetic configuration. As presented in Fig. 1(e), the magnetic structure of $Mn_{3.5}Co_{0.5}N$ at low temperature can be viewed as two magnetic sublattices: one with a FM arrangement and the other with a canted AFM structure (which yields a FM component antiparallel to the FM sublattice). This configuration is thus analogous to the interface caused by FM/AFM heterostructures but with a smaller net magnetic moment. In this structure, the magnetic anisotropy of the AFM sublattice is supposed to be dominant compared to the FM sublattice one and to the exchange coupling between the two sublattices. As a result, when cooled in an external magnetic field, the FM spins rotate according to the external field while the AFM spins remain in the original configuration. However, the canted AFM sublattice generates a non-null magnetic field that is imposed on the FM sublattice, leading to the incomplete reversal of FM spins. This small net magnetic moment will act like the pinned spins in the conventional EB model and will cause the VMS as well as the EB effect.[20] This may also explain why only a relatively small cooling field is enough to increase substantially the EB.

The role of the Co substitution at the corner site of the Mn_3AX lattice can be examined by comparing $Mn_{3.5}Co_{0.5}N$ with other antiperovskite systems where A is occupied by non-magnetic atoms or Mn.[25–28] The active contribution of Co is dual: first, the presence of magnetic ions at the corner site

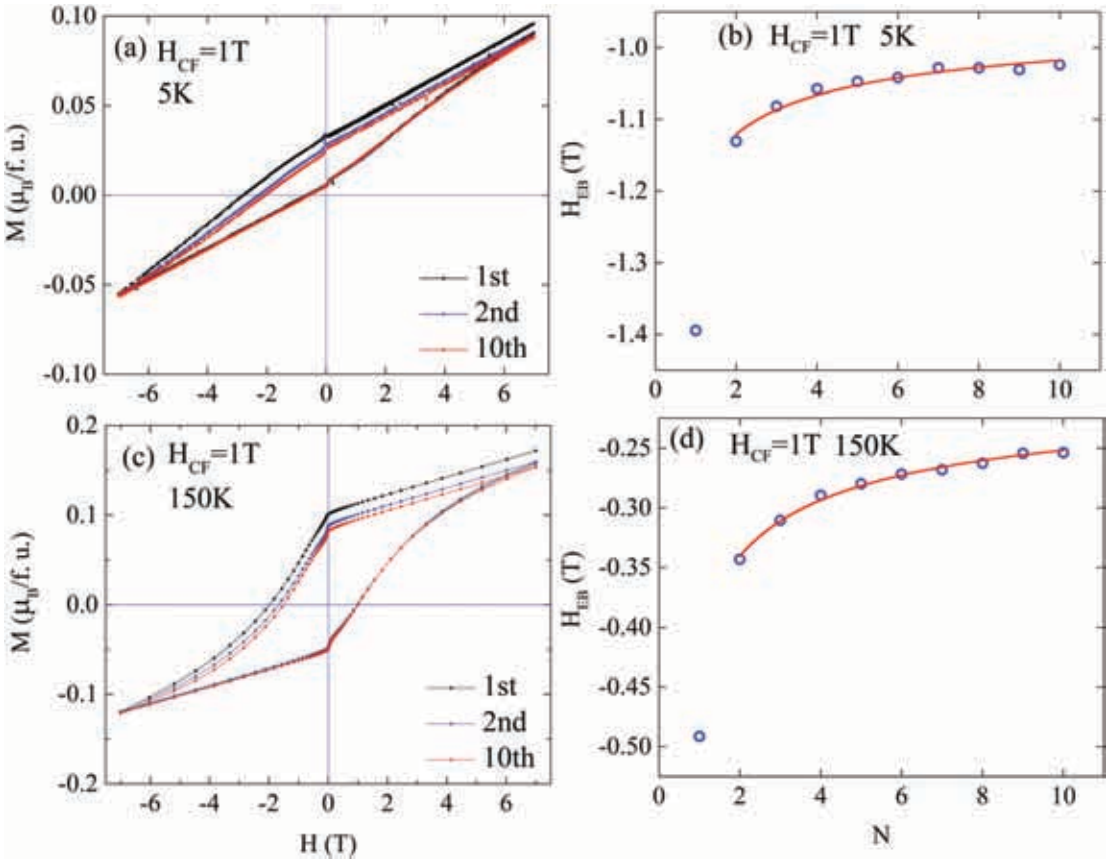

Fig. 5 Training effect of $Mn_{3.5}Co_{0.5}N$. Consecutive hysteresis loops measured at 5 K (a) and 150 K (c) after field cooling under 1 T. H_{EB} as a function of cycling index number, N, at 5 K (b) and 150 K (d). Solid lines show the best fits with eqn (1) to the data for $N > 1$.

stabilizes the collinear FIM structure observed below T_C as also reported in the Mn_4N parent compound; and second, the unique role of Co is to reduce the exchange interactions between the two sublattices and to allow the second AFM transitions associated with mGM4+ noncollinear magnetic structures. These simple observations put forward new insights into the material design of antiperovskites for giant EB around room temperature. A promising way of probing this concept would be the substitution of elements such as Fe and Ni or other non-magnetic elements for Mn^{II} in Mn_4N (T_N = 745 K) in order to decrease the exchange interactions between the two sublattices allowing the EB effect.[40] Bearing in mind technological applications, our work also proposes a promising opportunity to realize giant exchange bias in a single thin film of $Mn_{3.5}Co_{0.5}N$ rather than a conventional complex heterostructure, avoiding the complication and difficulty in the preparation of high quality interfaces.

4 Conclusions

To conclude, we have found a giant EB effect, up to −1.2 T after a FC procedure with a small applied field of 500 Oe, and a large H_{EB} = −0.28 T in the ZFC procedure under T_N = 256 K in $Mn_{3.5}Co_{0.5}N$. Neutron diffraction reveals that $Mn_{3.5}Co_{0.5}N$ first undergoes a FIM transition at T_C = 400 K, then a complex AFM phase transition with noncollinear spin arrangements occurs at 256 K. The latter phase is responsible for the generation of both ZFC and FC exchange bias effects due to the global interaction between two magnetic sublattices, as well as the observed large NTE behaviour. The strong correlation between VMS and exchange bias lays out a distinct approach to yield exchange bias in single phase materials. These findings provide new avenues for exploiting advanced magnetic materials and devices.

5 Experimental methods

5.1 Sample preparation and characterization

Polycrystalline samples of $Mn_{3.5}Co_{0.5}N$ were synthesized through solid-state reactions between Mn_2N and Co powders with an excess of Co. The reaction powders were carefully mixed, ground and pressed into pellets. The pellets were wrapped in Ta foils and sealed under vacuum ($P < 10^{-5}$ Pa) into quartz tubes. An excess of cobalt is needed to counterbalance the losses due to the reaction between the Co and the Ta foil leading to the formation of $CoTa_2$. Then, the pellets were sintered at 800 °C for 80 h, and cooled down to room temperature. Magnetic susceptibilities were measured using SQUID-VSM magnetometers (Quantum Design, MPMS3) between 5 and 400 K under a magnetic field of 0.1 T under both zero-field-cooled (ZFC) and field-cooled (FC)

conditions. Magnetic hysteresis loops were measured at different temperatures using the SQUID-VSM magnetometer from −7 T to 7 T under ZFC and FC conditions. The heat capacity was recorded between 2 and 300 K on cooling at 0 T employing a pulse relaxation method using a commercial calorimeter (Quantum Design PPMS).

5.2 Neutron diffraction experiments

Neutron powder diffraction (NPD) experiments were carried out at the ISIS pulsed neutron and muon facility of the Rutherford Appleton Laboratory (UK), on the WISH diffractometer located at the second target station.[45] Powder samples (2 g) were loaded into 6 mm cylindrical vanadium cans and measured in the temperature range of 5–550 K using a Closed Cycle Refrigerator (CCR). Rietveld refinements of the crystal and magnetic structures were performed using the Fullprof program against the data measured in detector banks at average 2θ values of 58°, 90°, 122° and 154°, each covering 32° of the scattering plane.[37] Group theoretical calculations were done using the BasIreps, ISODISTORT and Bilbao Crystallographic Server (Magnetic Symmetry and Applications) software.[38,39]

Conflicts of interest

There are no conflicts to declare.

Acknowledgements

Lei Ding acknowledges the support from the Rutherford International Fellowship Programme (RIFP). This project has received funding from the European Union's Horizon 2020 research and innovation programme under the Marie Skłodowska-Curie grant agreements No. 665593 awarded to the Science and Technology Facilities Council. Lihua Chu acknowledges the support from the National Natural Science Foundation of China (NSFC) (No. 11504107). We acknowledge the help received during material characterizations from the Materials characterization laboratory at the ISIS facility.

Notes and references

1 W. H. Meiklejohn and C. P. Bean, *Phys. Rev.*, 1957, **102**, 1413.
2 J. Nogues, J. Sort, V. Langlais, V. Skumryev, S. Surinach, J. S. Munoz and M. D. Baro, *Phys. Rep.*, 2005, **422**, 65.
3 V. Skumryev, S. Stoyanov, G. H. Y. Zhang, D. Givord and J. Nogues, *Nature*, 2003, **423**, 850.
4 M. Gibert, P. Zubko, R. Scherwitzl, J. Iniguez and J. M. Triscone, *Nat. Mater.*, 2012, **11**, 195.
5 R. Morales, Z. P. Li, J. Olamit, K. Liu, J. M. Alameda and I. K. Schuller, *Phys. Rev. Lett.*, 2009, **102**, 097201.
6 S. Gider, B. U. Runge, A. C. Marley and S. S. P. Parkin, *Science*, 1998, **281**, 797.
7 J. Nogues and I. K. Schuller, *J. Magn. Magn. Mater.*, 1999, **192**, 203.
8 F. Radu, R. Abrudan, I. Radu, D. Schmitz and H. Zabel, *Nat. Commun.*, 2012, **3**, 725.
9 M. Huijben, P. Yu, L. W. Martin, H. J. A. Molegraaf, Y. H. Chu, M. B. Holcomb, N. Balke, G. Rijnders and R. Ramesh, *Adv. Mater.*, 2013, **25**, 4739.
10 D. A. Gilbert, J. Olamit, R. K. Dumas, B. J. Kirby, A. J. Grutter, B. B. Maranville, E. Arenholz, J. A. Borchers and K. Liu, *Nat. Commun.*, 2016, **3**, 725.
11 E. Lage, C. Kirchhof, V. Hrkac, L. Kienle, R. Jahns, R. Knochel, E. Quandt and D. Meyners, *Nat. Mater.*, 2012, **11**, 523.
12 W. Kuch, L. I. Chelaru, F. Offi, J. Wang, M. Kotsugi and J. Kirschner, *Nat. Mater.*, 2006, **5**, 128.
13 P. Miltenyi, M. Gierlings, J. Keller, B. Beschoten, G. Guntherodt, U. Nowak and K. D. Usadel, *Phys. Rev. Lett.*, 2000, **84**, 4224.
14 F. Nolting, A. Scholl, J. Stohr, J. W. Seo, J. Fompeyrine, H. Siegwart, J. P. Locquet, S. Anders, J. Luning, E. E. Fullerton, M. F. Toney, M. R. Scheinfein and H. A. Padmore, *Nature*, 2000, **405**, 767.
15 R. L. Stamps, *J. Phys. D: Appl. Phys.*, 2000, **33**, R247.
16 B. M. Wang, *et al.*, *Phys. Rev. Lett.*, 2011, **106**, 077203.
17 J. Nogues, C. Leighton and I. K. Schuller, *Phys. Rev. B: Condens. Matter Mater. Phys.*, 2000, **61**, 1315.
18 H. Ohldag, A. Scholl, F. Nolting, E. Arenholz, S. Maat, A. T. Young, M. Carey and J. Stohr, *Phys. Rev. Lett.*, 2003, **91**, 017203.
19 S. Giri, M. Patra and S. Majumdar, *J. Phys.: Condens. Matter*, 2011, **23**, 073201.
20 S. J. Yuan, L. Li, T. F. Qi, L. E. DeLong and G. Cao, *Phys. Rev. B: Condens. Matter Mater. Phys.*, 2013, **88**, 024413.
21 A. K. Nayak, M. Nicklas, S. Chadov, C. Shekhar, Y. Skourski, J. Winterlik and C. Felser, *Phys. Rev. Lett.*, 2013, **110**, 127204.
22 P. Liao, *et al.*, *Appl. Phys. Lett.*, 2014, **104**, 092410.
23 Y. H. Xia, *et al.*, *Phys. Rev. B*, 2017, **96**, 064440.
24 A. K. Nayak, *et al.*, *Nat. Mater.*, 2015, **14**, 679.
25 K. Takenaka and H. Takagi, *Appl. Phys. Lett.*, 2005, **87**, 261902.
26 K. Takenaka and H. Takagi, *Appl. Phys. Lett.*, 2009, **94**, 131904.
27 X. Y. Song, *et al.*, *Adv. Mater.*, 2011, **23**, 4690.
28 C. Wang, *et al.*, *Phys. Rev. B: Condens. Matter Mater. Phys.*, 2012, **85**, 220103.
29 L. Ding, C. Wang, Y. Y. Na and L. H. Chu, *Scr. Mater.*, 2011, **65**, 687.
30 J. Tan, *et al.*, *Nano Res.*, 2015, **8**, 2302.
31 J. C. Lin, P. Tong, W. Tong, S. Lin, B. S. Wang, W. H. Song, Y. M. Zou and Y. P. Sun, *Appl. Phys. Lett.*, 2015, **106**, 082405.
32 L. H. Chu, L. Ding, C. Wang, M. C. Li, Y. J. Gao and Z. H. Liu, *Materials*, 2018, **11**, 286.
33 L. Ding, C. Wang, L. H. Chu, J. Yan, Y. Y. Na, Q. Z. Huang and X. L. Chen, *Appl. Phys. Lett.*, 2011, **99**, 251905.
34 L. Ding, C. Wang, Y. Sun, C. V. Colin and L. H. Chu, *J. Appl. Phys.*, 2015, **117**, 213915.
35 D. Matsunami, A. Fujita, K. Takenaka and M. Kano, *Nat. Mater.*, 2015, **14**, 73.
36 S. H. Deng, *et al.*, *Chem. Mater.*, 2015, **27**, 2495.

37 J. Rodriguez-Carvajal, *Physica B*, 1993, **192**, 55–69.
38 B. J. Campbell, H. T. Stokes, D. E. Tanner and D. M. Hatch, *J. Appl. Crystallogr.*, 2006, **39**, 607.
39 J. M. Perez-Mato, S. V. Gallego, E. S. Tasci, L. Elcoro, G. de la Flor and M. I. Aroyo, *Annu. Rev. Mater. Res.*, 2015, **45**, 217.
40 W. J. Takei, R. R. Heikes and G. Shirane, *Phys. Rev.*, 1962, **125**, 1893.
41 Z. H. Liu, X. J. Z. Y. J. Zhang, H. G. Zhang and X. Q. Man, *Appl. Phys. Lett.*, 2016, **109**, 032408.
42 X. D. Tang, W. H. Wang, W. Zhu, E. K. Liu, G. H. Wu, F. B. Meng, H. Y. Liu and H. Z. Luo, *Appl. Phys. Lett.*, 2010, **97**, 242513.
43 J. Sharma and K. G. Suresh, *Appl. Phys. Lett.*, 2015, **106**, 072405.
44 Y. Sun, J. Z. Cong, Y. S. Chai, L. Q. Yan, Y. L. Zhao, S. G. Wang, W. Ning and Y. H. Zhang, *Appl. Phys. Lett.*, 2013, **102**, 172406.
45 L. Chapon, *et al.*, *Neutron News*, 2011, **22**, 22.